U. Rist[+]

DNS of Boundary-Layer Instability and Transition using the Spatial Approach

Abstract

Starting with the work of Fasel (1976), the research group at the University of Stuttgart has developed numerical methods for the realistic Direct Numerical Simulation of controlled laminar-turbulent transition in boundary layers using the spatial model. This paper presents results of K-type transition simulations in zero and adverse pressure gradients. Subsequently it is shown that such simulations can also be used for boundary layers in 'real-life' aeronautical applications, such as airfoils. For such a flow, the influence of steady suction at the wall is investigated and compared with experimental data.

Introduction

Laminar-turbulent transition in boundary layers plays a significant role in many practical applications. For instance, delaying the onset of transition on an aircraft wing reduces the skin friction drag, thus decreasing the fuel consumption of the airplane. Airfoils with a large portion of laminar flow based on a design that avoids strong adverse pressure gradients are only feasible for small aircraft, operating at relatively low Reynolds numbers where no wing sweep is necessary. Larger and faster aircraft need laminar flow control (LFC) devices to enforce laminar flow. Designing and optimizing such devices undoubtedly requires a good knowledge of the transition mechanisms.

Transition in boundary layers is a spatially evolving complex process influenced by many parameters, such as free-stream turbulence, Reynolds number, pressure gradient, etc. In order to reduce the number of these parameters, transition research has focussed on so-called 'controlled' transition in simple model flows, like, for instance, the flat-plate boundary layer. In such experiments, some kind of a wave maker is used to excite disturbances in the boundary layer. The streamwise evolution of these disturbances is then examined using, for instance flow visualization and hot-wire measurements.

In addition to experimental and theoretical work, Direct Numerical Simulations (*DNS*) based on the solution of the complete Navier-Stokes equations have played an increasingly important role in transition research during the past decade. The basic approach is similar to that of controlled experiments. Some regular perturbations are introduced into the integration domain, and their subsequent unstable, nonlinear development is computed. Two basically different kinds of numerical models have been used until the beginning of the 1990s, the 'temporal' and the 'spatial' model. The advantages and disadvantages of both

models are not reviewed here, they have already been discussed elsewhere (cf. Fasel, 1990, Kleiser & Zang, 1991).

In the spatial model the streamwise evolution of disturbances is simulated in a fixed integration domain extending over a large downstream distance. With this model, realistic simulations of controlled experiments are possible, even in flows with large streamwise gradients including feedback by local flow reversal. However, elaborating a properly working numerical method for this model is a difficult task due to the boundary conditions and high demands on numerical stability and accuracy.

Today, the computationally less demanding temporal model with its underlying unphysical assumptions has been widely supplanted by the spatial model. The numerical results obtained by the research group of H. Fasel at the University of Stuttgart, for instance, compare favorably well with available theoretical and experimental data. The vibrating-ribbon experiments of Kachanov (1987) for the fundamental breakdown in a Blasius boundary layer simulated by Rist and the nonlinear development of a three-dimensional wave packet according to the wave-packet experiments by Gaster & Grant (1975) simulated by Konzelmann proved to be the first successful DNS of controlled transition experiments using the spatial approach (see Fasel, 1990).

This paper presents some results of two of the major investigations performed in the past several years at the University of Stuttgart: K-type transition in boundary layers with zero and adverse pressure gradient. It is then shown that these simulations can be easily extended to LFC studies in boundary layers of 'real-life' airfoils including suction at the wall.

Numerical Model

The latest version of the DNS-scheme originally developed by Fasel (1976), extended to three-dimensions by Fasel *et al.* (1990), improved by Kloker *et al.* (1993) and by Kloker (1993), is described here. Only a general outline of the numerical model is given; details are available in the mentioned references and in Rist & Fasel (1995). Many of the basic features of our numerical scheme (disturbance flow formulation, 'relaminarization zone' at the outflow boundary, forcing at the wall, pseudo-spectral formulation, high-order finite difference discretizations, explicit time integration, etc.) are equally applicable for other flows, like separated flows, free shear layers, compressible boundary layers, 3D boundary layers, and Taylor-Couette flow, for example.

The basic configuration of the integration domain for boundary layers is relatively simple. As shown in Fig. 1, a finite rectangular box is selected to represent a certain region of the flow over a flat plate. The integration domain extends in streamwise direction from $x = x_0$ to $x = x_N$, covering typically more than ten Tollmien-Schlichting wave lengths, and y_u is chosen to cover approximately three boundary layer thicknesses (δ) at the outflow boundary. In the spanwise direction, the flow is assumed to be periodic with a chosen fundamental wavelength λ_z.

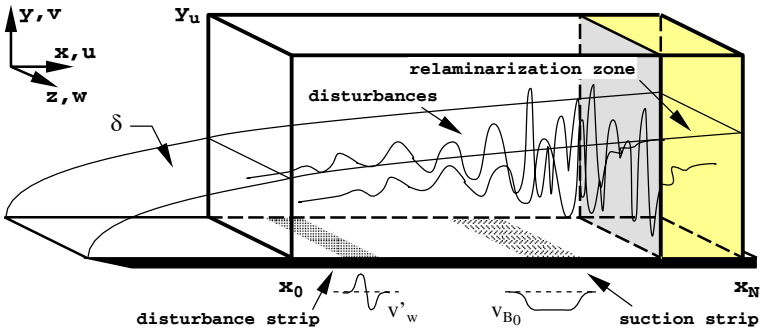

Figure 1: Integration domain.

Governing Equations

The numerical method is based on the three-dimensional Navier-Stokes equations for incompressible flow in vorticity-velocity formulation. The vorticity components are denoted by ω_x, ω_y and ω_z, and u, v and w are the velocity components in the x, y and z directions, respectively (see Fig. 1).

The equations are split into a set of equations for a two-dimensional steady base flow and a three-dimensional disturbance flow, i.e., for all variables $f = [u, v, \ldots, \omega_z]$ we have $f(x, y, z, t) = f_B(x, y) + f'(x, y, z, t)$. This allows the calculation of different base flows by prescribing different free-stream velocity distributions without altering the boundary conditions for the calculation of the disturbance flow. Thus, for investigations of the effects of different streamwise pressure gradients or steady suction at the wall, only a new base flow needs to be computed and specified for the calculation of the disturbance flow. The base flow is calculated from the 2D Navier-Stokes equations, *i.e.*, one vorticity-transport equation and two Poisson equations for the velocity components. The disturbance flow is described by three vorticity-transport equations and three Poisson equations for the velocity components. The detailed set of equations can be found in Fasel *et al.* (1990), Kloker *et al.* (1993) or Rist & Fasel (1995), for instance.

Boundary Conditions

An arbitrary streamwise pressure gradient can be imposed on the base flow by prescribing the streamwise velocity distribution $U_e(x)$ of the external flow at the free-stream boundary of the base flow calculation. Three different base flows are considered in this paper, one with $U_e(x) = 1$ (Blasius boundary layer), one with $U_e(x) = (x/x_0)^{-0.0826}$ (strongly decelerated Falkner-Skan boundary layer with Hartree parameter $\beta_H = -0.18$), and one where $U_e(x)$ is taken from an experiment to represent the velocity distribution of an airfoil. In any case the vorticity at the free-stream boundary is set to zero and $\partial v_B/\partial y = -dU_e/dx$ is specified for the calculation of v_B.

At the inflow boundary, Falkner-Skan profiles ($\equiv$ Blasius profiles for $\beta_H = 0$) corresponding to the imposed distribution of the streamwise pressure gradient are specified for the *base flow* variables. For a flow that does not belong to the Falkner-Skan family, as the airfoil boundary layer for instance, the streamwise velocity component $u_B(y)$ is taken from the Falkner-Skan velocity profile corresponding to the local pressure gradient and the local displacement thickness. Then, the $v_B(y)$ profile is integrated by using the continuity equation. At the outflow boundary, all equations are solved neglecting the second derivatives with respect to x, i.e., the equations are parabolized in the streamwise direction. At the wall, the velocity components are zero, except for the suction strip. The effect of suction through a porous strip is simulated by prescribing a normal velocity distribution $v_{B,0}(x)$ at the wall as sketched in Fig. 1.

A detailed description of the boundary conditions used for the calculations of the three-dimensional *disturbance flow* is given by Fasel *et al.* (1990), Kloker *et al.* (1993), and Rist & Fasel (1995). At the wall, all disturbance velocity components are zero, except within the disturbance strip, where the normal velocity component v'_w can be prescribed as a function of x, z, and t in order to introduce controlled time-periodic 2-D and 3-D disturbance waves. At the free-stream boundary, vanishing vorticity fluctuations and an exponential decay of the velocity disturbances are assumed. At the inflow boundary, all velocity and vorticity disturbances are set to zero. A harmonic wave condition in x-direction is applied at the outflow boundary. In addition, an artificial suppression of disturbances is introduced in the 'relaminarization zone' upstream of the outflow boundary (see Fig. 1) to substantially reduce the disturbance level at this boundary (cf. Kloker *et al.*, 1993 for details). Thus, possible undue reflections caused by large amplitude, broad-band disturbances passing the outflow boundary are prevented.

Numerical Method

For the numerical solution of both the base flow and the disturbance flow equations a fourth-order accurate finite-difference discretization is employed in the streamwise direction and normal to the wall, which allows for a proper treatment of the effects of the spatially varying boundary layer. The discretization in the spanwise direction for the disturbance flow is done by using a Fourier series

$$f'(x,y,z,t) = \sum_{k=-K}^{K} F_k(x,y,t)\, e^{ik\gamma z} \tag{1}$$

to exploit the periodicity with respect to z, where the complex $F_k = [U_k, V_k, \ldots, \Omega_{zk}]$ represent all disturbance variables in spectral space, and γ is the basic spanwise wavenumber defined by $\gamma = 2\pi/\lambda_z$.

For the base flow, the vorticity-transport equation is integrated by a semi-implicit Euler scheme in artificial time until convergence to a steady state is achieved. For the disturbance flow, the integration in time is performed by an

explicit four-stage Runge-Kutta scheme of fourth-order accuracy. The time integration is coupled with a fourth-order accurate discretization of the x-convection terms using central, upwind, downwind, and again central finite differences in each of the four stages, respectively. The sequence of upwind and downwind differences is altered for every time step. It can be shown that this technique effectively damps out small-scale oscillations that cannot be accurately discretized on a given grid at no additional computational cost (Kloker, 1993). The V_k-Poisson equation is solved with a multi-grid method using SOR line iteration technique (LU-decomposition in y, iteration in x). The equations for U_k and W_k are reduced to ODEs and directly solved.

Numerical Results

As already stated, the numerical simulation is performed in two steps. First, the steady two-dimensional base flow is calculated, i.e., a boundary layer under combined effect of streamwise pressure gradient and local suction through a narrow suction strip (if necessary). Second, two- and three-dimensional disturbance waves with prescribed frequency and amplitude are introduced into the domain by periodic blowing and suction through a narrow disturbance strip at the wall (shown schematically in Fig. 1). After several periods of forcing, the streamwise evolution of these disturbances can be observed in the unsteady numerical results like in a wind tunnel experiment.

Using periodic disturbance input, a periodic wave train is generated which travels downstream as sketched in Fig. 1. The numerical method was carefully validated by extensive comparisons with results from linear (spatial) stability theory, secondary instability theory and experiments (Fasel *et al.*, 1990).

K-type Transition

DNS of the K-type controlled transition experiments by Kachanov *et al.* (1985) have been performed by Rist (cf. Rist & Fasel, 1995), using $K = 8$ in equation (1), and extensively compared with the available experimental data (Kachanov, 1987 & 1994). In order to document the good agreement of the DNS with the experiments, new comparisons for later stages of transition are shown here in Figures 2 to 4 using data computed by Kloker (1993) with $K = 15$.

In Figure 2, u'-rms amplitudes are shown together with amplitudes (A_h) and phases (ϕ_h) from a Fourier decomposition of the x-velocity component $u(x, y, z, t) = \sum_h A_h(x, y, z) \cos[h f_1 t - \phi_h(x, y, z)]$, where f_1 is the fundamental disturbance frequency. The direct quantitative comparison of the DNS results with experimental data for $\tilde{y} = 4$ mm at the spanwise 'peak' and 'valley' stations in Fig. 2(a) and (b) shows excellent agreement. It should be noted here that only the disturbance amplitudes of the 2D TS-wave and its spanwise modulation at the disturbance strip placed at $x = 250$ mm were adjusted in such a way that the experimental amplitudes at $x = 300$ mm were closely met.

Two regions can be distinguished in the results for the 'peak' station: a rather

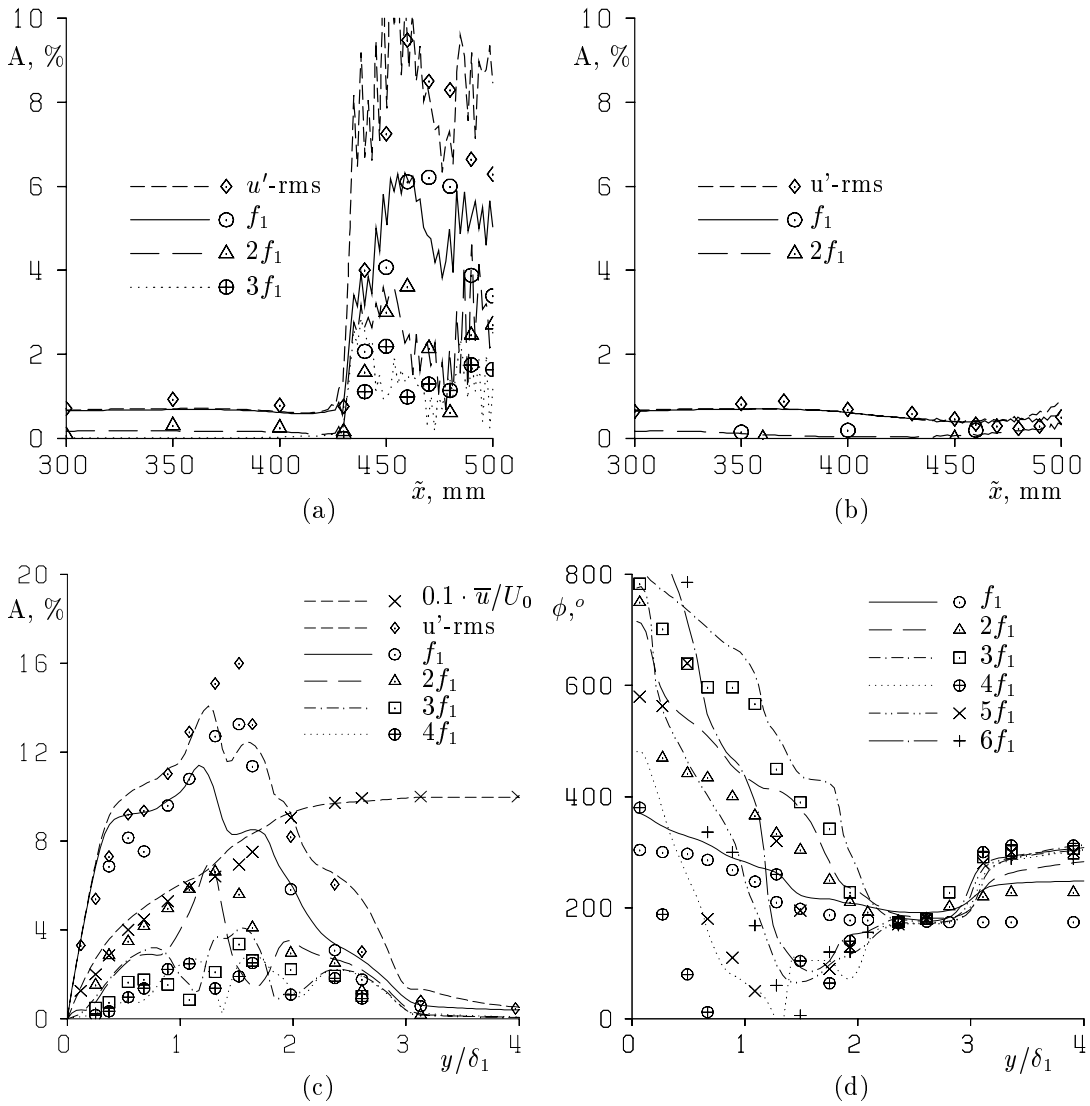

Figure 2: Comparison of u'-disturbances. Lines = DNS, symbols = experimental measurements by Kachanov *et al.* (1985), f_1 = disturbance frequency.

(a) amplitude (A) at $\tilde{y} = 4$ mm, z at 'peak'

(b) amplitude (A) and mean flow ($\overline{u}$) at $\tilde{y} = 4$ mm, z at 'valley'

(c) amplitude (A) at $\tilde{x} = 450$ mm, z at 'peak'

(d) phase profile (ϕ) at $\tilde{x} = 450$ mm, z at 'peak'

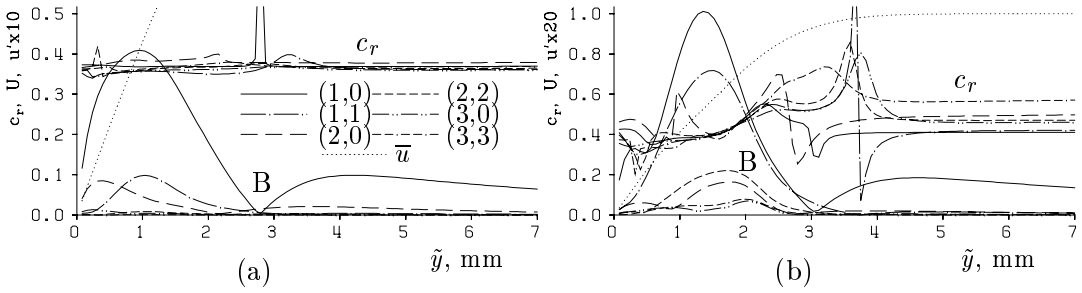

Figure 3: Comparison of phase speeds c_r with mean-velocity $\overline{u}$ and spectral amplitudes B for various frequency–spanwise-wave-number modes $(h,\ k)$. **a.** $\tilde{x} = 350$ mm, **b.** $\tilde{x} = 410$ mm.

modest weakly nonlinear disturbance development upstream of $\tilde{x} \approx 430$ mm, followed by a highly nonlinear region with several 'spikes' per disturbance cycle. The sudden increase of the peak rms- and higher-harmonic amplitudes is due to these spikes which are cut for $\tilde{x} \geq 430$ mm. Fig. 2(c) and (d) show a quantitative comparison of the amplitude and phase profiles, respectively for the highly nonlinear 'two-spike stage' at $\tilde{x} = 450$ mm which also exhibits a remarkable agreement. The first spike is situated between $y/\delta_1 = 2.4$ and 2.8 ($\tilde{y} \approx 4$ mm) where the phases are equal to 180^o due to their normalization with respect to the passage of the first spike.

In figures 3 and 4 the disturbances are examined in the frequency–spanwise-wave-number spectrum defined by $u(x,y,z,t) = \sum_h \sum_k B_{h,k}(x,y)\cos[k\gamma z - hf_1 t - \theta_{h,k}(x,y)]$. The phase speeds $c_{rh,k} = hf_1/(\partial\theta_{h,k}/\partial x)$ of the modes (h,k) in Figure 3 exhibit new, interesting features. Upstream of $\tilde{x} \approx 400$ mm, the phase speeds versus y are practically constant and all modes are phase-locked to the 2D wave. Thus, the disturbances show 'wave-like' behavior and the flow field in this stage is defined by nonlinear waves. Figure 3 clearly shows that the nonlinear interaction is not confined to the critical layer (i.e., the y-position where the mean flow $\overline{u}$ equals the phase speed): Except for mode (1,0), all phase speeds are significantly different from their linear values due to the phase lock observed above. In addition, there is no observable increase of higher harmonic amplitudes in the critical layer by nonlinear interactions. Only the fundamental 2D and 3D disturbance amplitudes [modes(1,0) and (1,1)] exhibit a maximum in the critical layer, but this is already there in the linear case.

Further downstream in the spike stage, shown in Fig. 3(b), the 'wave-like' behavior disappears: the phase speeds change with respect to y, especially inside the boundary layer. Outside, they are no longer phase-locked. At this stage it is much more difficult to define a critical layer and to attribute a special nonlinear significance to it. The only distinct feature that can be observed is a region of equal phase speed at $\tilde{y} \approx 2$ mm where the first spike is just being formed. Since spikes are the manifestation of small Ω-shaped vortices, we suppose that this part of the flow field must be governed by nonlinear dynamic interactions of

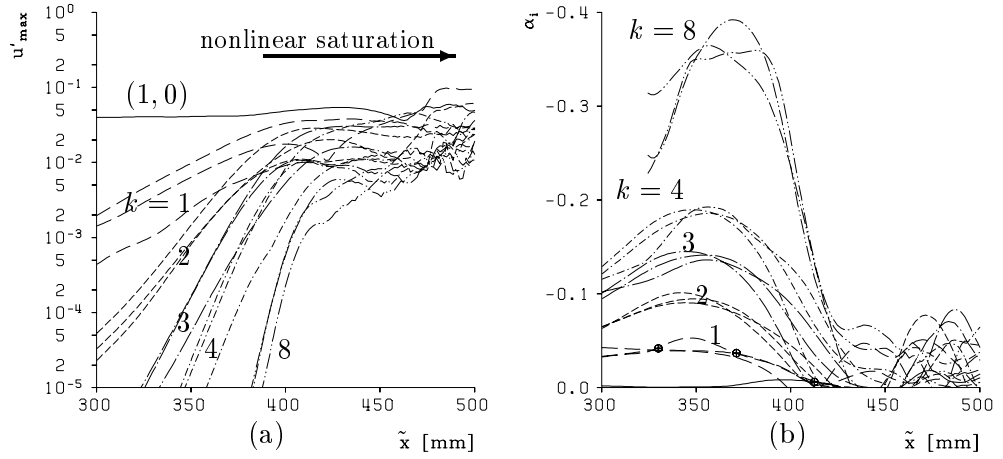

Figure 4: Amplitude maxima (a) and amplification rates α_i (b) for various spectral modes: frequencies $0, f_1, 2f_1$, spanwise wave numbers $k = 1, 2, 3, 4, 8$. ($\oplus$) = Floquet theory, Fasel *et al.* (1988).

local fluid-flow structures in contrast to the wave interactions in the first sector.

Both regimes also appear in Figure 4 where the y-maxima of the B-amplitudes defined above and the amplification rates $\alpha_i = -d/dx(B_{max})$ are shown for various frequency–spanwise-wave-number modes $[(h, k), 0 \leq h \leq 2, k > 0]$ versus x. It is quite evident that the initial amplification rates of the spanwise higher harmonics grow (linearly) with the spanwise wave number for $\tilde{x} < 400$ mm. The initial fan-out and deviation from linear increase of the modes with $k = 3, 4, 8$ should not be considered, since these modes are initially affected by the numerical round-off error due to their extremely small amplitudes ($B_{max} < 10^{-6}$) for small x.

Comparisons of the amplification rates α_i with an extension of Herbert's (1988) secondary instability theory are also shown. They reveal that the amplification of modes (1,1) and (1,0) is due to a 'combined' subharmonic-fundamental resonance with the 2D modes (1,0) and (2,0) (Fasel *et al.*, 1988). The possibility whether or not such a resonance could amplify other modes as well has also been checked. It turned out that α_i due to secondary instability is largest for $k = 1$, so that the modes with higher k must be considered as higher harmonic disturbance components of the fundamental disturbances. This hypothesis has been further checked in a number of test calculations using different initial amplitudes for these modes. It turned out that the local amplitudes (and amplification rates) of the higher harmonics do not depend on their initial disturbance amplitude but on the local amplitude of the waves that are amplified by the 'combined' resonance. Thus, it appears that this resonance is the kernel that drives the flow through the first stage of K-type transition.

In the second stage, nonlinear effects lead to a saturation of all amplitudes on a high level as can be observed in Fig. 4. So far, no wave resonances could be

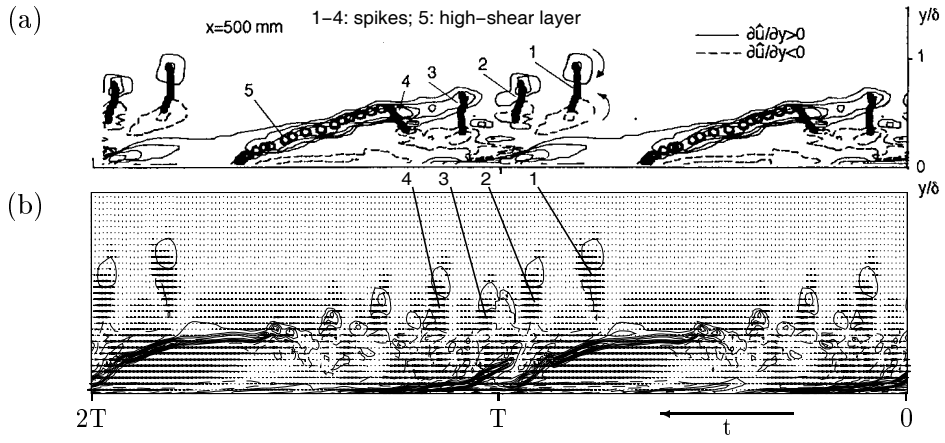

Figure 5: Experimental (a) and numerical (b) contours of $\partial u'/\partial y$ at $\tilde{x} = 500$ mm. (b) together with u'.

discovered in the numerical data. This absence might be due to the appearance of local dynamics that apparently replace the 'wave-like behavior' observed in the first regime.

Simulations of the late-stage structures downstream of $\tilde{x} = 450$ mm have been started recently using $K = 64$ in eq. (1), see Rist & Kachanov (1994). Figure 5 shows a comparison of the instantaneous shear $\partial u'/\partial y$ at $\tilde{x} = 500$ mm for the peak station from the DNS with data from Kachanov (1994). Spikes and a high-shear layer close to the wall are mapped out by black dots and circles, respectively in the experimental data. Regions of large negative u' indicate spikes in the numerical results. Instead of only four in the experiment, five or six spikes can be observed in the DNS. Besides that, the qualitative features in both data sets are identical: a high-shear layer traversing the entire boundary layer and several spikes (Ω-vortices) at its downstream end. However, there is no doubt that further analysis of these new data is required to learn more about possible interactions of such structures with the near-wall region, for instance.

Application to a Boundary Layer with Adverse Pressure Gradient

Kloker (1993) has used a Falkner-Skan-type boundary layer with Hartree parameter $\beta_H = -0.18$ for comparison with the K-type simulation in the previous section. At first glance the results look very much like those for the Blasius boundary layer (cf. Figure 6). Aligned Λ-vortices are forming out of a spanwise modulation of the large-amplitude TS-wave and Ω-vortices appear together with spikes at the spanwise peak stations. The downstream disturbance development, however, although quite similar in the peak plane, is drastically more violent at the spanwise valley station in the case with adverse pressure gradient than with zero pressure gradient (Kloker & Fasel, 1995). A closer look at the results in-

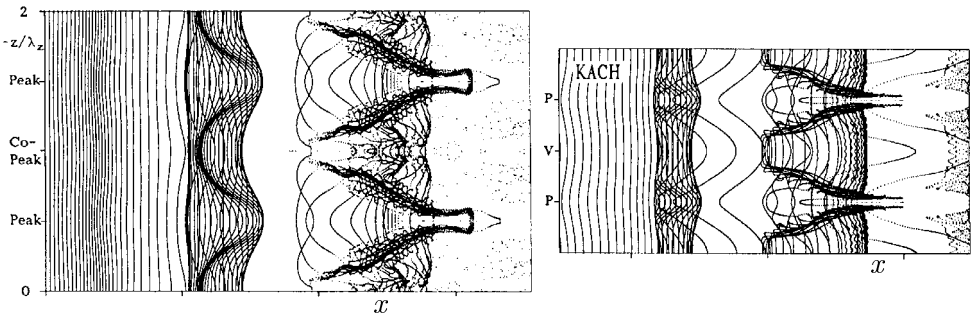

Figure 6: Simulated time-lines. Comparison betweeen adverse pressure gradient (left) and zero pressure gradient boundary layer (right).

dicated that the breakdown occurs much earlier there than at the peak station. This is why Kloker called this station a 'Co-Peak' station instead of 'Valley'. A new secondary vortex system close to the wall, centered around this station, induces a (lower) quite characteristic high-shear layer in between neighbouring Λ-vortices and accelerates transition at the 'Co-Peak' station. This event proceeds much more rapidly than the formation and breakdown of the well-known (upper) high-shear layer on top of the Λ-vortex. These violent dynamic events are apparent in Fig. 6 but could be perceived much better in an animation.

Application to an Airfoil with Suction

The base flows of wind-tunnel experiments on a NACA 64_2-A-215 airfoil with suction performed by van Ingen (1965) have been calculated. Between 30% and 90% of the airfoil chord (c) the wing section has been divided into 20 suction chambers, each of which was adjustable separately in order to prevent flow separation with only minimal viscous drag by suction through a porous surface. Bestek *et al.* (1994) have simulated this flow by prescribing the velocity distribution shown in Fig. 7(a) at the free-stream boundary of the integration domain. Two calculations have been performed: one without suction at the wall with the integration domain reaching from $s/c = 0.2$ to 0.55, and one with the suction velocity of van Ingen extending to $s/c = 0.72$.

Fig. 7(b) shows a comparison of the DNS results with the experiments for the streamwise distributions of the displacement thickness δ_1 and the momentum thickness δ_2 for both cases. Without suction the strong growth of both indicates the inclination to separation. For the suction case, δ_1 and δ_2 grow only moderately. For both cases, the numerical and experimental results are in good agreement. The neglection of the airfoil surface curvature in the numerical model is justified due to the small ratio of boundary-layer thickness to surface curvature radius within the considered chord region. Thus, the basis for subsequent simulations of disturbance control in practical applications is prepared.

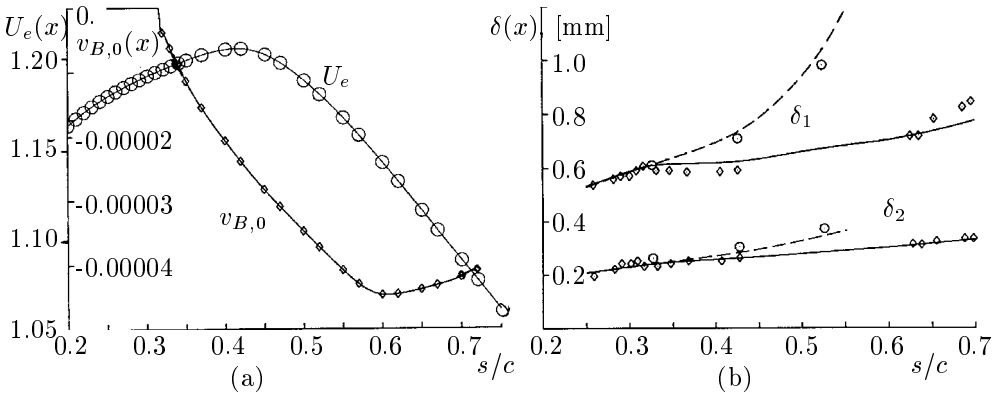

Figure 7: (a) Free-stream velocity U_e and wall-suction velocity $v_{B,0}$ for the DNS of a NACA 64_2-A-215 airfoil boundary layer with suction. (b) Comparison of boundary layer growth. Symbols = experiments v. Ingen (1965).

Conclusions

A numerical method has been developed and optimized over the past several years that can now be used to perform high-resolution spatial DNS of instability and transition in various boundary-layers of practical interest, provided a high-performance, large-memory computer is available. The results shown here demonstrate a good quantitative agreement with available experimental data. Research within the next few years must focus on flow control in such flows, on boundary-layer receptivity, and on understanding the late-stage structures of transition to turbulence in 2D as well as in 3D mean flows.

Acknowledgements

The work reviewed here would have been impossible without the long-term funding by the Deutsche Forschungsgemeinschaft, the Stiftung Volkswagenwerk, the Bundesministerium für Forschung und Technologie, the generous support of computer time provided by the University of Stuttgart, and continuous stimulation by its initiator Hermann Fasel.

References

Bestek, H., Kloker, M. & Müller, W. 1994 - Spatial direct numerical simulation of boundary layer transition under strong adverse pressure gradient. AGARD-Symposium *Application of Direct and Large Eddy Simulation to Transition and Turbulence*, Chania, Crete, Greece, AGARD-CP 551, pp. 32-1–32-12.

Fasel, H.F. 1976 - Investigation of the stability of boundary layers by a finite-difference model of the Navier-Stokes equations. *J. Fluid Mech.* **18**, 355–383.

Fasel, H.F. 1990 - Numerical simulation of instability and transition in boundary-layer flows. In: *Laminar-Turbulent Transition* (D. Arnal and R. Michel, eds),

Springer, Berlin, pp. 587–598.
Fasel, H.F., Rist, U. & Konzelmann, U. 1988 - Numerical investigation of the effects of longitudinal vortices on the onset of transition in a flat-plate boundary layer. AGARD-Symposium *Fluid Dynamics of Three-Dimensional Shear Flows and Transition*, Cesme, Turkey, AGARD-CP 438, pp. 7-1–7-13.
Fasel, H.F., Rist, U. & Konzelmann, U. 1990 - Numerical investigation of the three-dimensional development in boundary-layer transition. *AIAA J.* **28**, 29–37.
Gaster, M. & Grant I. 1975 - An experimental investigation of the formation and development of a wave packet in a laminar boundary layer. *Proc. Roy. Soc. London A* **341**, 253–269.
Herbert, T. 1988 - Secondary instability of boundary layers. *Ann. Rev. Fluid Mech.* **20**, 487–526.
Ingen van, J.L. 1965 - Theoretical and experimental investigations of incompressible laminar boundary layer with and without suction. TU Delft, Report VTH–**124**.
Kachanov, Y.S. 1987 - On the resonant nature of the breakdown of a laminar boundary layer. *J. Fluid Mech.* **184**, 43–74.
Kachanov, Y.S. 1994 - Physical Mechanisms of laminar-boundary-layer transition. *Ann. Rev. Fluid Mech.* **26**, 411–482.
Kachanov, Y.S., Kozlov, V.V., Levchenko, V.Y. & Ramazanov, M.P. 1985 - On nature of K-breakdown of a laminar boundary-layer; new experimental data. In: *Laminar-Turbulent Transition* (V.V. Kozlov ed.), Springer, Berlin, pp. 61–73.
Kleiser, L. & Zang T.A. 1991 - Numerical Simulation of Transition in Wall-Bounded Shear Flows. *Ann. Rev. Fluid Mech.* **23**, 495–537.
Kloker, M. 1993 - Direkte numerische Simulation des laminar-turbulenten Strömungsumschlages in einer stark verzögerten Grenzschicht. Dissertation, Univ. Stuttgart.
Kloker, M., & Fasel, H.F. 1995 - Direct numerical simulation of boundary-layer transition with strong adverse pressure gradient. In: *Laminar-Turbulent Transition* (R. Kobayashi ed.), Springer, Berlin, pp. 481–488.
Kloker, M., Konzelmann, U. & Fasel, H.F. 1993 - Outflow boundary conditions for spatial Navier-Stokes simulations of transitional boundary layers. *AIAA J.* **31**, 620–628.
Rist, U. & Fasel, H.F. 1995 - Direct numerical simulation of controlled transition in a flat-plate boundary layer. *J. Fluid Mech.* **298**, 211–248.
Rist, U. & Kachanov, Y.S. 1995 - Numerical and experimental investigation of the K-regime of boundary-layer transition. In: *Laminar-Turbulent Transition* (R. Kobayashi ed.), Berlin, pp. 405–412.

[+]Institut für Aerodynamik und Gasdynamik
Universität Stuttgart
Pfaffenwaldring 21, 70550 Stuttgart, Germany